Effect of a metal artifact reduction algorithm on dehiscence and fenestration detection around zirconia implants with cone beam computed tomography

Bernardo Barbosa Freire, DDS, MSc, PhD,[a] Victor Aquino Wanderley, DDS, MSc, PhD,[b] João Victor Frazão Câmara, DDS, MSc,[c] Lethycia Almeida Santos, DDS, MSc,[d] Carolina Ruis Ferrari, DDS,[d] Tamara Teodoro Araujo, DDS, MSc,[d] and Israel Chilvarquer, DDS, MSc, PhD[a]

Objective. To assess the efficacy of the metal artifact reduction algorithm (MARA) of the Cranex 3D cone beam computed tomography (CBCT) device in the detection of peri-implant dehiscence and fenestration around zirconia implants.

Study Design. In total, 60 implants were placed in bovine ribs. Dehiscence and fenestration defects were created around the implants, after which 60 CBCT images were obtained with and 60 without activation of MARA. Three radiologists examined the images for the presence of defects. The area under the curve (AUC) from receiver operating characteristic analysis, sensitivity, and specificity were calculated to assess the ability to discriminate the presence vs absence of bone defects. One-way analysis of variance was employed to analyze outcome measures. The significance level was established at 5% ($\alpha = 0.05$).

Results. AUC values indicated excellent discrimination of dehiscence on images with MARA activation and an excellent to outstanding range of discrimination with MARA deactivation. For fenestration, MARA activation and deactivation both led to outstanding discrimination. Sensitivity and specificity values revealed that activation of MARA was helpful in distinguishing the presence vs. absence of dehiscence, while both MARA conditions were helpful for fenestration. However, there were no statistically significant differences between MARA activation and deactivation for any outcome measure ($P > .05$).

Conclusion. CBCT is suitable for detecting peri-implant defects, but MARA application does not significantly affect peri-implant dehiscence and fenestration detection. (Oral Surg Oral Med Oral Pathol Oral Radiol 2024;138:316−323)

Rehabilitation treatment using dental implants in completely or partially edentulous patients has been practiced on a large scale by the dental profession, driven by the increase in technical and scientific knowledge gained in implant dentistry. Currently, titanium implants are widely used due to their excellent biocompatibility, good mechanical properties, and long-term clinical success.[1] Although titanium is a popular material, it has the drawback of being gray in color, which can darken the gingival tissue in significantly thin biotypes.[2] Another disadvantage is related to the galvanic reaction of titanium implants, which is an electrochemical process that can occur after the implant body comes into contact with saliva and fluoride, resulting in an inflammatory response that can lead to alveolar bone resorption.[3]

The evolution of dental materials and technological systems has enabled the development of dental implants made of zirconia. These implants have proven to be suitable for rehabilitation concerning such requirements as biocompatibility, mechanical characteristics, and aesthetic properties related to their white color.[4] Nevertheless, incorrect positioning of dental implants can bring about complications such as dehiscence and peri-implant fenestration. Dehiscence occurs when there is an absence of bone from the cervical portion of the implant, while fenestration is characterized by the absence of bone over part of the implant but where the cervical portion has bone coverage.[5] Early diagnosis of a bone defect in the buccal and/or lingual cortex of the anterior region of the maxilla and mandible is extremely important for maintaining the function and aesthetics of the implants.

Statement of Clinical Relevance

Early diagnosis of defects in cortical bone around zirconia dental implants is important for maintaining function and aesthetics. Cone beam computed tomography is suitable for detecting peri-implant defects, but metal artifact reduction algorithms do not significantly affect diagnostic outcomes.

[a]Department of Stomatology, School of Dentistry, University of São Paulo, São Paulo, Brazil.
[b]Department of Clinical and Preventive Dentistry, Federal University of Pernambuco, Recife, Brazil.
[c]Clinic of Operative Dentistry, Periodontology and Preventive Dentistry, Saarland University Hospital, Saarland University, Homburg, Saarland, Germany.
[d]Department of Biological Sciences, Bauru School of Dentistry, University of São Paulo, Bauru, Brazil.
Corresponding author: João Victor Frazão Câmara. E-mail address: jvfrazao92@hotmail.com
Received for publication Aug 29, 2023; returned for revision Jan 31, 2024; accepted for publication Feb 18, 2024.

2212-4403/$-see front matter
https://doi.org/10.1016/j.oooo.2024.02.023

Intraoral radiographic techniques have the drawback of a 2-dimensional representation of the radiographed structures; these images are therefore contraindicated for detecting peri-implant bone defects.[6,7] The disadvantage of 2D imaging can be resolved by using cone beam computed tomography (CBCT), which depicts the region of interest without superimposition of other structures. CBCT enables satisfactory evaluation of the buccal and lingual cortical bone.[8] A comprehensive publication in 2020 detailed the extensive array of CBCT devices currently available on the market (approximately 203 devices), listing variations in combinations of kilovoltage, milliamperage, focal spot size, detector type, contrast resolution, spatial resolution, and reconstruction algorithm that characterize the variations in performance of these units.[9] Despite these differences, artifacts are always present in CBCT images and pose significant challenges to interpretation and diagnosis. Beam-hardening artifacts are a type of error or distortion in the reconstructed data caused by the absorption of low-energy X-ray photons when interacting with dense objects that have high atomic numbers, consequently increasing the mean energy of the X-ray beam. These artifacts often obscure diagnostically important structures and are directly related to the atomic number of the metallic material and its size, quantity, and location.[10,11]

Metal artifact reduction algorithms (MARAs) have been introduced by some manufacturers to correct this artifact in CBCT images. MARAs identify and minimize the streaking and dark banding artifacts in the scanned volume. These algorithms typically function by interpolating or replacing the distorted projection data with estimated gray values, thereby improving image quality.[12] The usage of MARA remains a controversial subject in the literature. While some studies recommended its application,[13,14] others did not discover efficacy for diagnostic performance in the detection of dehiscence or fenestration.[12] However, when evaluating the published research on the effectiveness of MARAs, it is important to highlight the methodological variations, such as the type of dental material utilized, the specific type of MARA applied, and the diversity of CBCT systems, all of which could contribute to the alteration of subjective perception of image artifacts.[15]

Thus, the present study aimed to compare the detection of peri-implant dehiscence and fenestration defects in bovine ribs containing a zirconia abutment implant by examining images acquired with the Cranex 3D CBCT unit (Soredex) with and without application of the MARA. The null hypothesis tested was that no significant differences would be identified in the detection of dehiscence and fenestration through MARA activation vs deactivation.

MATERIALS AND METHODS

Ethical aspects

This study was considered exempt by the Ethics Committee on Use of Animals (CEUA) of the School of Dentistry of the University of São Paulo (protocol number 022/2018).

Sample preparation

Bovine ribs donated by a slaughterhouse registered with the Brazilian Health Regulatory Agency (ANVISA) were used. The ribs were fragmented using a bandsaw. Fragments of fresh bovine ribs in good condition with bone thickness greater than 5.5 mm and height greater than 11 mm were included in the sample. Rib fragments with extensive bone surface irregularity, cortical bone disruption, and/or insufficient dimensions (height x width x thickness) for proper dental implant installation were excluded from the study. The rib fragments were stored in a container containing water to keep them hydrated.

The fragments were used as bone support to install dental implants as an alternative approach to placing implants in a dry human jaw. The sample was used to obtain CBCT images of 60 bovine rib fragments. One dental implant with integrated zirconia connections (Straumann PURE Ceramic System), with measurements of 4.1 mm wide x 10 mm high, was installed in each of the fragments.

Installation of implants

The dental implants were installed in the bovine ribs by the same implantologist, who used a Straumann surgical kit. Drills with diameters of 2.2 mm, 2.8 mm, 3.5 mm, and 4.2 mm were used in sequence, with motor and contra-angle in a reduction of 20:1 and torque of 45 N-cm. The touch ratchet was used to aid in installing the dental implants. The implantologist ensured that the procedure maintained the proximity between the dental implant and the cortical bone to guarantee the conditions of the peri-implant bone defects. Transillumination of the cortical bone in the surgical beds with a light-emitting diode was performed to ensure that the preparation was in close proximity to the cortex.

Bone defect induction

After the dental implants were installed in the bovine ribs, peri-implant bone defects of dehiscence and fenestration were created in the cortical bone adjacent to the implant by using a low-speed spherical drill. Dehiscence was induced at the cervical bone margin of the implant and had a 2.5 mm diameter and semielliptical shape. Fenestration was induced in the bone region adjacent to the apical third of the dental implant and had a 2.5 mm diameter and circular shape.[12] The defects were all created on the surface of the rib fragment that faced the x-ray beam (i.e., the “buccal” surface).

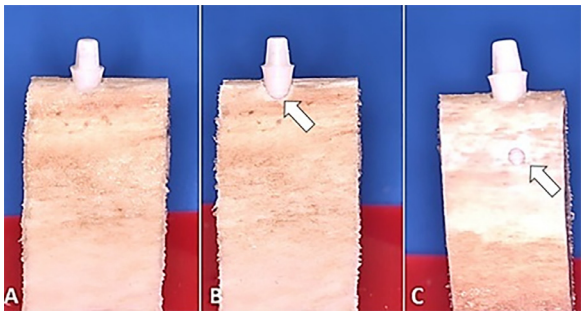

Fig. 1. Zirconia implants in bovine rib fragments. A) Control with no peri-implant defect. B) Peri-implant dehiscence (arrow) at the cervical bone margin of the implant with a 2.5 mm diameter and semi-elliptical shape. C) Peri-implant fenestration (arrow) adjacent to the apical third of the dental implant with a 2.5 mm diameter and circular shape.

The 60 rib fragments with dental implants were divided into 3 groups: (1) 20 specimens with no peri-implant bone defects (controls), (2) 20 specimens with dehiscence, and (3) 20 samples with fenestration (Figure 1).

Acquisition of CBCT images

CBCT scans were obtained using the Cranex 3D unit operating at 90 kV, 8 mA, voxel size of 0.13 mm^3, field of view (FOV) of 4 cm x 4 cm, and acquisition time of 19 s. Each bone fragment was positioned in the unit on a leveling platform at the appropriate height and standardized by using the luminous guidelines of the equipment, so that the entire specimen was located inside the FOV. The fragments were immersed individually inside a circular plastic container with water to simulate X-ray attenuation in the soft tissues around bone.[16]

CBCT images of each of the 60 bone fragments (20 controls, 20 with dehiscence, and 20 with fenestration) were acquired under 2 different conditions: (1) with MARA activated and (2) with MARA deactivated. As a result, 120 tomographic volumes were obtained. Examples of images from each group acquired with MARA activation and deactivation are shown in Figure 2.

Image analysis

The acquired images were randomized and made available for independent examination by 3 dental radiology specialists, each with over 5 years of experience in CBCT evaluation. The examiners received a document that explained the purpose of the study, assessment period, diagnostic scores to be applied to the images, and format for filling out the worksheets. They were

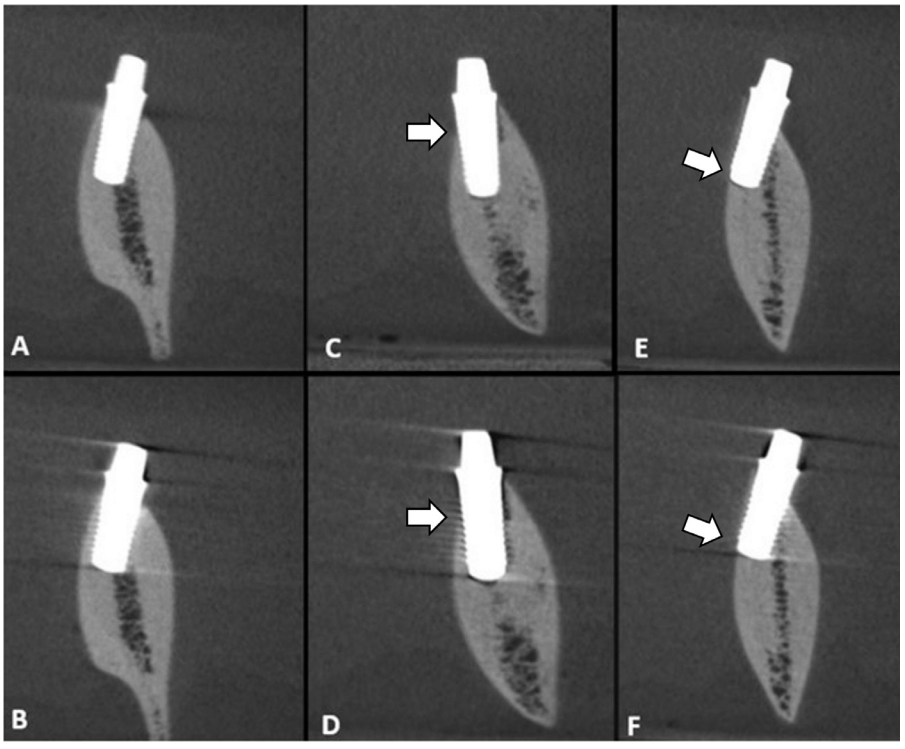

Fig. 2. Cone beam computed tomography images of bovine rib fragments representing each of the 3 groups of rib fragments with the metal artifact reduction algorithm (MARA) activated and deactivated. A) Control with MARA activated. B) Control with MARA deactivated. C) Dehiscence (arrow) with MARA activated. D) Dehiscence (arrow) with MARA deactivated. E) Fenestration (arrow) with MARA activated. F) Fenestration (arrow) with MARA deactivated.

trained to use the CBCT OnDemand3D software (Cybermed) and were familiarized with the imaging procedure. The examinations were conducted in a dimly illuminated room. The examiners analyzed the entire dataset acquired from each of the 120 CBCT volumes in the axial, coronal, and sagittal planes and were allowed to use the brightness, contrast, and zoom tools.

The examiners, working independently, were instructed to record their confidence in the presence or absence of cortical bone dehiscence or fenestration according to a 5-point scale: 1, definitely absent; 2, probably absent; 3, uncertain; 4, probably present; and 5, definitely present. Forty percent of the sample was reassessed by the examiners 30 days after the initial evaluations were concluded to ascertain intraexaminer reproducibility. The data were tabulated on a Microsoft Office Excel 2013 spreadsheet (Microsoft Corporation), and analyzed using SPSS software version 22 (IBM Corporation).

Statistical analysis

The ability of the examiners to discriminate between the presence and absence of dehiscence and fenestration defects on CBCT images captured with activation and deactivation of the MARA device was calculated as the area under the curve (AUC) generated by each examiner through receiver operating characteristic (ROC) analysis. The AUC outcomes were assessed using the scale proposed by Hosmer et al.,[17] in which 0.5-0.7 indicates poor discrimination; 0.7-0.8, acceptable discrimination; 0.8-0.9, excellent discrimination; and greater than 0.9, outstanding discrimination.

The outcome measures of sensitivity and specificity were also calculated. For this, the data were dichotomized, with scores 1 and 2 representing a negative finding (absence of a bone defect) and scores 4 and 5 representing a positive finding (presence of a bone defect). Since no examiners entered a score of 3 (uncertain) as a response, it was discarded. For a test to be useful, the sum of sensitivity and specificity should be at least 1.5 (halfway between 1, which is useless, and 2, which is perfect).[18] The reference standard for all examinations was the known status of the presence or absence of a bone defect on each of the 60 bone fragments. The statistical significance of differences in diagnosing both dehiscence and fenestration with MARA activation vs deactivation was assessed for AUC and all other outcome measures with one-way analysis of variance (ANOVA). The significance level was set at 5% ($\alpha = 0.05$).

After data collection, the inter- and intraexaminer agreement rates of the 3 examiners were determined by using the weighted kappa index. The level of agreement was interpreted according to the scale of Landis and Koch,[19] in which kappa values of 0.00-0.20 indicate bad agreement; 0.21-0.40, reasonable agreement; 0.41-0.60, moderate agreement; 0.61-0.80, good agreement; and 0.81-1.00, excellent agreement.

RESULTS

The AUC values from the evaluations of the 3 examiners for detecting dehiscence and fenestration with and without MARA activation are shown in Table I. For detection of dehiscence, excellent discrimination ability was found on images with MARA activation, with AUC values ranging from .86 to .88, while there was an excellent to outstanding range of discrimination with MARA deactivation (.81-.91). On the other hand, outstanding discrimination ability for fenestration detection was observed with both MARA activation (0.94-0.96) and deactivation (0.92-0.96). There were no statistically significant differences between MARA activation and deactivation in diagnosing dehiscence ($P = .38$) or fenestration ($P = .99$).

Table II summarizes the mean values of sensitivity and specificity obtained by the 3 examiners for dehiscence and fenestration detection with MARA activation vs deactivation. For dehiscence, the sum of sensitivity and specificity was 1.566 with activation, indicating that MARA application was helpful in distinguishing the presence vs. absence of the lesion, but deactivation of MARA diminished the value of the exam (sum = 1.48). On the other hand, the scans were successful in distinguishing the presence of fenestration from normal cases both with and without MARA application, since the sum of sensitivity and specificity was 1.616 with MARA activated and 1.650 with MARA deactivated. There were no statistically significant differences for these diagnostic tests regarding the activation or deactivation of the MARA tool ($P > .05$).

Interexaminer agreement for dehiscence with MARA activation ranged from good to excellent, with

Table I. Area under the curve values from receiver operating characteristic analysis by each examiner for dehiscence and fenestration detection with activation and deactivation of the metal artifact reduction algorithm (MARA)

	Examiner	*MARA activation*	*MARA deactivation*
Dehiscence	1	0.87	0.91
	2	0.88	0.87
	3	0.86	0.81
	Average (SD)	0.87 (0.01)	0.86 (0.03)
Fenestration	1	0.96	0.92
	2	0.96	0.96
	3	0.94	0.94
	Average (SD)	0.95 (0.01)	0.94 (0.02)

Table II. Mean sensitivity and specificity for dehiscence and fenestration detection with activation and deactivation of the metal artifact reduction algorithm (MARA)

		MARA activation	*MARA deactivation*
Dehiscence	Sensitivity	0.716	0.65
	Specificity	0.85	0.83
	Sum	1.566	1.48
Fenestration	Sensitivity	0.683	0.667
	Specificity	0.933	0.983
	Sum	1.616	1.650

weighted kappa values of .75-.85, but agreement on images with MARA deactivation was considered good (.73-.78). Interexaminer agreement for fenestration ranged from good to excellent with both MARA activation (.74-.87) and deactivation (.80-.87). Intraexaminer agreement for dehiscence with MARA activation ranged from good to excellent, with kappa values of .75-.91, while with MARA deactivation it was considered excellent (.88-1.00). Intraexaminer agreement for fenestration with MARA activation ranged from good to excellent, with kappa values of .73-.97, while agreement on images with MARA deactivation was considered excellent (.87-1.00), as listed in Table III.

DISCUSSION

Implant-supported prosthetic rehabilitation has expanded across a wider socioeconomic range in recent years as treatment costs have declined. The more common use of implant therapy has raised challenging diagnostic issues in clinical practice.[19] The presence of peri-implant bone defects can compromise rehabilitation treatment. In these cases, clinical symptoms trigger the search for a diagnosis, often using periapical radiographs as an initial evaluation method. However, because these images are 2-dimensional, they lack information on details of the bone support structure on the buccal and lingual regions of the dental implant.[20–24] Hence, CBCT examination may play an important role in acquiring the information that facilitates the diagnosis of bone defects, since the 3-dimensional visualization of the tomographic volume guarantees an analysis without distortion and superimposition of structures.[26] CBCT also provides the ability to make linear measurements that allow the objective assessment of bone loss, which may present decisive information for diagnosis and selection of the most appropriate surgical correction approach, including bone grafts.[25]

Studying the diagnosis of peri-implant bone defects is of utmost importance in dentistry because the constant development of technology ultimately improves the quality of images, thereby enhancing the diagnostic accuracy of clinicians.[18] Although acquisition protocols that use the metal artifact reduction algorithm as a tool have been recommended, studies are scarce that evaluate peri-implant bone defect diagnosis for zirconia implants, considering that these diagnoses are made from images with a greater number of artifacts.[26,27]

The diagnostic studies of peri-implant bone defects presented in the literature for evaluating dehiscence and fenestration mention the use of titanium dental implants in their methodology. In their evaluation of the effectiveness of MARAs in detecting peripheral bone defects using bovine ribs with titanium implants, De-Azevedo-Vaz et al.[12] obtained better results in diagnostic values for fenestration and observed no significant difference with activation of MARA, thus corroborating the findings of the present study. Although they used a dried skull instead of beef ribs in their methodology, Kolsuz et al.[28] also found no significant difference with MARA activation, and observed better results in the diagnostic values for the fenestration bone defect.

Research has demonstrated the usefulness of MARAs in improving the accuracy of diagnosing dehiscence and fenestration around dental implants, but these studies were based on the use of titanium implants.[29] Our investigation to test the variable of MARA status in the detection of peri-implant bone defects from zirconia abutment implants arose from the greater expression of artifacts caused by this material, and therefore represents an innovative and unique approach. This differentiation in the choice of implant material brings significant novelty to the research, introducing a new and potentially transformative

Table III. Inter- and intraexaminer agreement for the presence of dehiscence and fenestration as detected on cone beam computed tomography images with activation and deactivation of the metal artifact reduction algorithm (MARA)

MARA	*Dehiscence*		*Fenestration*	
	Interexaminer	*Intraexaminer*	*Interexaminer*	*Intraexaminer*
Activation	0.79 (0.75-0.85)	0.85 (0.75-0.91)	0.82 (0.74-0.87)	0.88 (0.73-0.97)
Deactivation	0.76 (0.73-0.78)	0.96 (0.88-1.00)	0.84 (0.80-0.87)	0.93 (0.87-1.00)

Weighted kappa values are presented as Mean (Min-Max).

perspective in the context of applying MARA for accurate diagnoses around dental implants. However, this factor was not enough to guarantee a significant difference in the number of artifacts.[30]

Kamburoglu et al.[31] investigated the accuracy of CBCT images with and without metal artifact reduction activation to detect periodontal bone defects and artificial peri-implantitis produced with a spherical bur. Higher values were observed for the diagnosis of periodontal defects than peri-implant bone defects. This may be directly related to the lower quality of dental implant images caused by artifacts. Furthermore, intra-examiner agreement was greater than the agreement between different examiners, corroborating the findings of the present study. This result is common in research with multiple examiners who have different experience levels and cognitive abilities. Nevertheless, no significant differences were observed in the diagnostic values in that study when the variable of MARA activation was tested. In the current investigation, however, it is important to highlight that for dehiscence, activation of MARA was helpful in distinguishing the presence vs absence of the lesion, yielding a sum of sensitivity and specificity of 1.566, but inactivation of MARA diminished the value of the exam (sum = 1.48). On the other hand, the scans were successful in distinguishing the presence of fenestration from normal cases both with and without MARA activation, since the sum of sensitivity and specificity exceeded 1.5 for both conditions.

The difference in the methodologies of diagnostic studies of peri-implant bone defects may be related to the different bone structure support; the different ways of inducing the bone defect; and the different imaging modalities, equipment, and procurement protocols.[32] A relevant point to be considered when observing the values of CBCT diagnostic tests is the spatial resolution of these images. According to the acquisition protocol selected by the radiologist and provided by the equipment, images can be obtained with different spatial resolutions. It is known that CBCT images can accurately determine the thickness of the cortical bone adjacent to implants, especially with high-resolution protocols in which the acquisition voxels are small.[33]

De-Azevedo-Vaz et al.[34] evaluated the accuracy of CBCT in diagnosing dehiscence and fenestration by comparing 2 different voxel sizes (0.2 mm^3 and 0.12 mm^3). The scans with the smaller voxels did not improve the results, in contrast with study expectations. The authors emphasized that the difference between the 2 voxel sizes was not sufficient to guarantee significant differences in diagnostic values. However, a technical issue that must be raised concerns the limitation of some CBCT devices in regard to acquisition protocol selection, where smaller voxels are inseparably associated with smaller FOVs. Higher spatial resolution associates acquisition protocols with a lower dose of radiation.

In contrast to the study by De-Azevedo-Vaz et al.,[34] who evaluated only 2 sizes of voxels on the same CBCT equipment, Kolsuz et al.[28] examined 6 different voxel sizes in 2 CBCT devices. The results suggested a voxel size of 0.15 mm^3 as a reference for diagnosing periodontal defects. Based on these previous studies, we believe that the acquisition protocol of the present research would be best for use in clinical examinations of peri-implant bone defects when using the Cranex 3D CBCT equipment.

Another important point brought up in the present investigation involved how periodontal bone defects were induced. Bagis et al.[35] asserted that the way bone defects are created can affect the diagnostic values of periodontal bone defects and recommended that defects be induced with a drill or with the combination of a drill and chemicals. We chose to induce bone defects mechanically in an acquisition protocol with a 4 cm x 4 cm FOV and 0.13 mm^3 voxel size, taking the ALADA concept of radioprotection (as low as diagnostically acceptable) into account. This concept relates the acquisition protocols to images with sufficient quality for diagnosis but with the lowest possible dose of radiation.

Future clinical studies should be performed with a greater number of variables since we showed no significant difference in the diagnostic values for detecting peri-implant bone defects in the presence of a zirconia implant abutment in CBCT images acquired with or without the activation of the metal artifact reduction algorithm.

CONCLUSION

Cone beam computed tomography was efficacious in allowing examiners to detect the presence of dehiscence and fenestration, with AUC scores in the good to outstanding range and sums of sensitivity and specificity exceeding 1.5 in most cases, but MARA activation status had no significant effect on outcomes.

DECLARATION OF INTEREST

None.

CREDIT AUTHORSHIP CONTRIBUTION STATEMENT

Bernardo Barbosa Freire: Conceptualization, Formal analysis, Investigation, Methodology, Resources, Software, Writing – original draft. **Victor Aquino Wanderley:** Investigation, Methodology, Writing – review & editing. **João Victor Frazão Câmara:** Investigation, Writing – review & editing. **Lethycia Almeida Santos:** Investigation, Methodology.

Carolina Ruis Ferrari: Investigation, Methodology. **Tamara Teodoro Araujo:** Investigation, Methodology. **Israel Chilvarquer:** Conceptualization, Data curation, Investigation, Methodology, Resources, Software, Supervision, Writing – original draft, Writing – review & editing.

REFERENCES

1. Jacobs R, Salmon B, Codari M, Hassan B, Bornstein MM. Cone beam computed tomography in implant dentistry: recommendations for clinical use. *BMC Oral Health*. 2018;18(1):88. https://doi.org/10.1186/s12903-018-0523-5.
2. Ottria L, Lauritano D, Andreasi Bassi M, et al. Mechanical, chemical and biological aspects of titanium and titanium alloys in implant dentistry. *J Biol Regul Homeost Agents*. 2018;32(2 Suppl. 1):81-90.
3. Li Y, Ling J, Jiang Q. Inflammasomes in alveolar bone loss. *Front Immunol*. 2021;12:691013. https://doi.org/10.3389/fimmu.2021.691013.
4. Zhang Y, Lawn BR. Novel zirconia materials in dentistry. *J Dent Res*. 2018;97(2):140-147. https://doi.org/10.1177/0022034517737483.
5. Schünemann FH, Galárraga-Vinueza ME, Magini R, et al. Zirconia surface modifications for implant dentistry. *Mater Sci Eng C Mater Biol Appl*. 2019;98:1294-1305. https://doi.org/10.1016/j.msec.2019.01.062.
6. Shanbhag S, Pandis N, Mustafa K, Nyengaard JR, Stavropoulos A. Bone tissue engineering in oral peri-implant defects in preclinical in vivo research: a systematic review and meta-analysis. *J Tissue Eng Regen Med*. 2018;12(1):e336-e349. https://doi.org/10.1002/term.2412.
7. Ocksrider J, Boden AL, Greif DN, et al. Radiographic evaluation of reconstructive surgery for segmental bone defects: what the radiologist should know about distraction osteogenesis and bone grafting. *Clin Imaging*. 2020;67:15-29. https://doi.org/10.1016/j.clinimag.2020.05.018.
8. Raes F, Renckens L, Aps J, Cosyn J, De Bruyn H. Reliability of circumferential bone level assessment around single implants in healed ridges and extraction sockets using cone beam CT. *Clin Implant Dent Relat Res*. 2013;15(5):661-672. https://doi.org/10.1111/j.1708-8208.2011.00393.x.
9. Gaêta-Araujo H, Alzoubi T, Vasconcelos KF, et al. Cone beam computed tomography in dentomaxillofacial radiology: a two-decade overview. *Dentomaxillofac Radiol*. 2020;49(8):20200145. https://doi.org/10.1259/dmfr.20200145.
10. Schulze R, Heil U, Gross D, et al. Artefacts in CBCT: a review. *Dentomaxillofac Radiol*. 2011;40(5):265-273. https://doi.org/10.1259/dmfr/30642039.
11. Ni X, Shi Z, Song X, et al. Metal artifacts reduction in kV-CT images with polymetallic dentures and complex metals based on MV-CBCT images in radiotherapy. *Sci Rep*. 2023;13(1):8970. https://doi.org/10.1038/s41598-023-35736-x.
12. de-Azevedo-Vaz SL, Peyneau PD, Ramirez-Sotelo LR, Vasconcelos Kde F, Campos PS, Haiter-Neto F. Efficacy of a cone beam computed tomography metal artifact reduction algorithm for the detection of peri-implant fenestrations and dehiscences. *Oral Surg Oral Med Oral Pathol Oral Radiol*. 2016;121(5):550-556. https://doi.org/10.1016/j.oooo.2016.01.013.
13. Queiroz PM, Groppo FC, Oliveira ML, Haiter-Neto F, Freitas DQ. Evaluation of the efficacy of a metal artifact reduction algorithm in different cone beam computed tomography scanning parameters. *Oral Surg Oral Med Oral Pathol Oral Radiol*. 2017;123(6):729-734. https://doi.org/10.1016/j.oooo.2017.02.015.
14. de Faria Vasconcelos K, Queiroz PM, Codari M, et al. A quantitative analysis of metal artifact reduction algorithm performance in volume correction with 3 CBCT devices. *Oral Surg Oral Med Oral Pathol Oral Radiol*. 2020;130(3):328-335. https://doi.org/10.1016/j.oooo.2020.03.049.
15. Wanderley VA, Leite AF, de Faria Vasconcelos K, et al. Impact of metal artefacts on subjective perception of image quality of 13 CBCT devices. *Clin Oral Investig*. 2022;26(6):4457-4466. https://doi.org/10.1007/s00784-022-04409-w.
16. Shelley AM, Brunton P, Horner K. Subjective image quality assessment of cross sectional imaging methods for the symphyseal region of the mandible prior to dental implant placement. *J Dent*. 2011;39(11):764-770. https://doi.org/10.1016/j.jdent.2011.08.008.
17. Hosmer DW Jr, Lemeshow S, Sturdivant RX. *Applied Logistic Regression*. 3rd ed. John Wiley & Sons; 2013:177. https://doi.org/10.1002/9781118548387.
18. Power M, Fell G, Wright M. Principles for high-quality, high-value testing. *Evid Based Med*. 2013;18(1):5-10. https://doi.org/10.1136/eb-2012-100645.
19. Landis JR, Koch GG. The measurement of observer agreement for categorical data. *Biometrics*. 1977;33(1):159-174.
20. Chen ZY, Gao S, Zhang YW, Zhou RB, Zhou F. Antibacterial biomaterials in bone tissue engineering. *J Mater Chem B*. 2021;9(11):2594-2612. https://doi.org/10.1039/d0tb02983a.
21. Bagegni A, Spies BC, Kern M, Hazard D, Kohal R. The influence of prosthetic crown height and implant-abutment connection design selection on the long-term implant-abutment stability: a laboratory study. *J Mech Behav Biomed Mater*. 2021;113:104095. https://doi.org/10.1016/j.jmbbm.2020.104095.
22. Bagegni A, Zabler S, Nelson K, et al. Synchrotron-based micro computed tomography investigation of the implant-abutment fatigue-induced microgap changes. *J Mech Behav Biomed Mater*. 2021;116:104330. https://doi.org/10.1016/j.jmbbm.2021.104330.
23. Bergamo ETP, Campos TMB, Piza MMT, et al. Temporary materials used in prosthodontics: The effect of composition, fabrication mode, and aging on mechanical properties. *J Mech Behav Biomed Mater*. 2022;133:105333. https://doi.org/10.1016/j.jmbbm.2022.105333.
24. Mota de Almeida FJ, Knutsson K, Flygare L. The effect of cone beam CT (CBCT) on therapeutic decision-making in endodontics. *Dentomaxillofac Radiol*. 2014;43(4):20130137. https://doi.org/10.1259/dmfr.20130137.
25. Kuusisto N, Huumonen S, Kotiaho A, Haapea M, Rekola J, Vallittu P. Intensity of artefacts in cone beam CT examinations caused by titanium and glass fibre-reinforced composite implants. *Dentomaxillofac Radiol*. 2019;48(2):20170471. https://doi.org/10.1259/dmfr.20170471.
26. Farias-Gomes A, Fontenele RC, Rosado LPL, Neves FS, Freitas DQ. The metal post material influences the performance of artefact reduction algorithms in CBCT images. *Braz Dent J*. 2022;33(1):31-40. https://doi.org/10.1590/0103-6440202204222.
27. Guilfoile C, Rampant P, House M. The impact of smart metal artefact reduction algorithm for use in radiotherapy treatment planning. *Australas Phys Eng Sci Med*. 2017;40(2):385-394. https://doi.org/10.1007/s13246-017-0543-5.
28. Kolsuz ME, Bagis N, Orhan K, Avsever H, Demiralp KÖ. Comparison of the influence of FOV sizes and different voxel resolutions for the assessment of periodontal defects. *Dentomaxillofac Radiol*. 2015;44(7):20150070. https://doi.org/10.1259/dmfr.20150070.
29. Sheikhi M, Behfarnia P, Mostajabi M, Nasri N. The efficacy of metal artifact reduction (MAR) algorithm in cone-beam computed tomography on the diagnostic accuracy of fenestration and dehiscence around dental implants. *J Periodontol*. 2020;91(2):209-214. https://doi.org/10.1002/JPER.18-0433.

30. Kerkfeld V, Meyer U. Higher Resolution in cone beam computed tomography is accompanied by improved bone detection in peri-implant bone despite metal artifact presence. *Int J Oral Maxillofac Implants*. 2018;33(6):1331-1338. https://doi.org/10.11607/jomi.6623.
31. Kamburoglu K, Kolsuz E, Murat S, Eren H, Yüksel S, Paksoy CS. Assessment of buccal marginal alveolar peri-implant and periodontal defects using a cone beam CT system with and without the application of metal artefact reduction mode. *Dentomaxillofac Radiol*. 2013;42(8):20130176. https://doi.org/10.1259/dmfr.20130176.
32. Demirturk Kocasarac H, Koenig LJ, Ustaoglu G, Oliveira ML, Freitas DQ. CBCT image artefacts generated by implants located inside the field of view or in the exomass. *Dentomaxillofac Radiol*. 2022;51(2):20210092. https://doi.org/10.1259/dmfr.20210092.
33. Razavi T, Palmer RM, Davies J, Wilson R, Palmer PJ. Accuracy of measuring the cortical bone thickness adjacent to dental implants using cone beam computed tomography. *Clin Oral Implants Res*. 2010;21(7):718-725. https://doi.org/10.1111/j.1600-0501.2009.01905.x.
34. de-Azevedo-Vaz SL, Vasconcelos Kde F, Neves FS, Melo SL, Campos PS, Haiter-Neto F. Detection of periimplant fenestration and dehiscence with the use of two scan modes and the smallest voxel sizes of a cone-beam computed tomography device. *Oral Surg Oral Med Oral Pathol Oral Radiol*. 2013;115(1):121-127. https://doi.org/10.1016/j.oooo.2012.10.003.
35. Bagis N, Eren H, Kolsuz ME, Kurt MH, Avsever H, Orhan K. Comparison of the burr and chemically induced periodontal defects using different field-of-view sizes and voxel resolutions. *Oral Surg Oral Med Oral Pathol Oral Radiol*. 2018;125(3):260-267. https://doi.org/10.1016/j.oooo.2017.11.010.